Draft: *Analytical Chemistry*, 2021, *93 (49)*, 16409-16416.

Electrochemical Beacon Method to Quantify Ten Attomolar of Nucleic Acids with Semi-Log Dynamic Range of Seven Orders of Magnitude

Rahul Tevatia[a],*, Alicia Chan[a], Lance Oltmanns[a], JayMin Lim[a], Ander Christensen[a], Michael Stoller[a], Ravi F. Saraf[b],[c]*

[a]Vajra Instruments, Lincoln, NE 68512, USA; [b]University of Nebraska, Lincoln, NE 68588, USA; [c]Nebraska Center for Material and Nanoscience, University of Nebraska-Lincoln, NE 68512

For Table of Contents Only

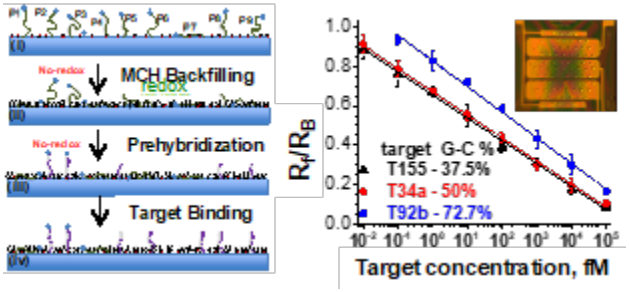

Electrochemical Beacon Method to Quantify Ten Attomolar of Nucleic Acids with Semi-Log Dynamic Range of Seven Orders of Magnitude

Rahul Tevatia[a],*, Alicia Chan[a], Lance Oltmanns[a], JayMin Lim[a], Ander Christensen[a], Michael Stoller[a], Ravi F. Saraf[b],[c]*

[a]Vajra Instruments, Lincoln, NE 68512, USA; [b]University of Nebraska, Lincoln, NE 68588, USA; [c]Nebraska Center for Material and Nanoscience, University of Nebraska-Lincoln, NE 68512

* rahul.tevatia@vajrainstruments.com; rsaraf2@unl.edu

ABSTRACT

Change in the dynamics of ssDNA or RNA probes tethered to Au electrode on immuno-specific binding to analyte is a versatile approach to quantify variety of molecules, such as, heavy metal ions, pesticides, proteins, and nucleic acids. A widely studied approach is electrochemical beacon method where redox of a dye attached to the probe decreases as its proximity to the underlying electrode changes on binding. The limit of quantification (LOQ) defined by the semi-log dependence of the signal on target concentration is in picomolar range. Here, a method was studied where, by differential reflectivity, multiple reactions were measured on a monolith electrode. An alternative contrast mechanism was discovered that led to an approach to enhance the LOQ to 10 attomolar and increase dynamic range to seven orders of magnitude, using similar probes and binding conditions. Quantitative analysis on sequences with G-C fraction ranging from 37% to 72% were studied. The approach will allow development of label-free, enzyme-free, microarray to detect biomolecules including nucleic acids and proteins on a single electrode at quantification from 10 aM to 0.1 nM with high specificity.

KEYWORDS

Biosensor; Electrochemical sensor; Microarray; Electrochemical Beacon; Differential reflectivity; Aptamer sensor, microRNA

INTRODUCTION

Single stranded DNA (ssDNA) tethered to Au electrode is a broad platform to develop highly specific electrochemical biosensors for wide range of analytes by measuring change in the interfacial property on binding.[1, 2] One pervasively studied principle is to detect the analyte by measuring the change in the molecular dynamics of the tethered ssDNA on binding.[3-5] The concept is a highly versatile platform where, the ssDNA sequence of the "DNA brush" can be engineered with complexities, such as, aptamers with hairpins,[6-8] to target small analytes such as, heavy ions[9-11] and organophosphorus pesticides,[12, 13] to larger biomolecules, such as, HER2 protein for breast cancer screening,[14] thrombin and cocaine,[15] interferon-gamma,[16] SARS-CoV-2 spoke glycoprotein,[17] and circulating biomolecules in blood.[18, 19] The change in chain dynamics can be conveniently measured as an active electrochemical signal by attaching a redox active compound, such as, methylene blue (MB)[20] or ferrocene (Fc)[21] to the free-end of the probe ssDNA. Because the electrochemical signal of binding depends on the proximity and accessibility of the redox reporter to the electrode, the platform strategy is referred to as "electrochemical beacon".[22]

In the simplest configuration, the fully unfolded probes are 10 to 50 nucleotide (nt) long and are usually modified at the 5'-end with a thio-group via a flexible spacer, for example, HS-$(CH_2)_6$-[ssDNA]-3', that can spontaneously bind to Au electrode via a strong Au-S bond. The alkyl-chain spacer provides the flexibility to enable efficient binding to the analyte.[23, 24] Typical coverage of the probes on the Au electrode is around 5 x 10^{12} molecules/cm^2, amounting to inter-chain spacing of ~4.5 nm which is comparable to end-to-end distance of the probe which for example, is ~5.5 nm for 40 nt chain.[25] Considering the footprint to be about the size of the persistence length of ~1.5 nm,[25] the rest of well over 50% of the area is passivated with an inert compound, the most popular one being mercaptohexanol (MCH).[26] With a fluorophore attached at the free-end of the probe ssDNA significant change in chain flexibility occurs that was leveraged to measure probe-target binding at a sensitivity of 10 pM.[27, 28] In an electrochemical analog, a systematic decrease in the redox signal of Fc and MB tethered at the free-end is leveraged to quantify binding of target nucleic acid (NA) also as low as ~10 picomolar (pM).[3, 4, 29]

The balance between coverage and its effect on conformation and accessibility of probe, and ultimately binding efficiency is delicate. Typically, coverage in DNA brush biosensor are in 10^{11} to 10^{13} probe molecules/cm^2,[4, 5] where, the interchain distance is 30 to 3 nm, respectively, which at higher coverage is comparable to their size.[25, 30] Several studies have shown that higher coverage, typically above 10^{13} molecules/cm^2 leads to lower binding efficiency, attributed to steric hindrance and electrostatic repulsion.[31-34] Thus, a coverage around 5x10^{12} molecules/cm^2 seems optimal.

The primary motivation to study this highly versatile electrochemical beacon sensing method is to improve its limit of quantification (LOQ) and dynamic range. As noted above, binding efficiency drops significantly above ~10^{13} molecules/cm^2. As a result, the LOQ for current methods is limited to nanomolar range to at most tens of picomolar range.[3, 28, 29, 35] Non-linear systematics up to 1 fM is possible using complex configuration with highly folded probe

ssDNA.[36] The dynamic range is typically less than three orders of magnitude,[35] which may be increased to five orders of magnitude using complex sandwich structure.[37] Considering the largely ignored aspects of the interaction between the ssDNA probe and the Au electrode, and the effect of backfilling, we discovered inevitable heterogeneous conformational states of the probe where not all binding will lead to a change (i.e., decrease) in redox signal. By regulating the heterogeneity of the probe conformation, we demonstrate that the LOQ can be enhanced by six orders of magnitude to 10 attomolar (aM) and obtain a dynamic range of seven orders of magnitude. Furthermore, the approach to measure redox allows easy multiplexing by measuring multiple redox reactions on a monolith electrode with measurement spot diameter of ~10 μm and sample volume of ~100 μL.

EXPERIMENTAL

Reagents and Buffers. Ultrapure Dnase/Rnase free water (Thermofischer Scientific, USA) was used to prepare all buffer solutions and other solution. Subsequently referred to as DI water. Prehybridization, hybridization and SEED analysis were done in 1X-MPBS (1M NaCl; 10 mM phosphate buffer, pH 7.2; 1mM $MgCl_2$) (Sigma Aldrich, USA). Probes with tethered MB and thiol group (Supporting Information(SI), Table S1) and targets (SI, Table S2) were purchased from Integrated DNA Technologies (IDT), USA. High purity 6-mercapto-1-hexanol (MCH) was purchased from Sigma Aldrich, USA.

Chip fabrication. Si chips (1 cm^2) with ~1000 nm thermal oxide with three Au electrodes (thickness 300 nm; dimensions 0.1 x 0.8 mm) were patterned for 200 μm diameter microwells (n=25) (SI, Figure S1) using positive photoresist, KL5315 (KemLabs, USA) lithography. Briefly, the chips were cleaned by sonication for 5 min each in acetone, water, and ethanol followed by O_2 plasma (at 500 mTorr, 125 W) for 2 min. The chips were blow-dried by compressed air through a 0.2 μm Millipore Filter. The positive photoresist was spin cast on the chips at 5,000 rpm for 60 sec to obtain a ~500-nm thick film. The chips was prebaked for 5 min at 115 °C. The film was exposed to xenon (Xe) light (300 W) for 3 min through a contact mask with a chromium (Cr) metalized pattern on quartz using a mask aligner (Suss MJB3, KarlSuss, USA). The chips were developed in tetramethylammonium hydroxide (TMAH) developer by sonication for 5 min followed by ~60 s wash in DI water. The chips were then exposed to O_2 plasma (60 W for 2 min) and hard baked at 180 °C for 1 hr. The resulting pattern on each electrode was an array of 200 μm microwells exposing the underlying Au electrode.

Probe immobilization. Typically, unless otherwise noted, 10 μM of probes (SI, Table S1) in 1 M phosphate buffer, pH 7.2 (Sigma Aldrich, USA) were immobilize the lithographed chips. In certain cases, the concentration was varied (Figure 1c) but buffer was the same. The spotted chips with respective ~100 nL of probe solutions were allowed to incubate in a humid environment at 21 °C for about 90 min to ensure that the drop does not evaporate or grow due to condensation. After immobilization, the chip was washed in 1mM Tris-Cl, pH 7.2.

Probe Coverage. The method to measure probe coverage is described in details in a previous publication.[38] Briefly, all 75 microwells were immobilized with a single concentration of P34a as described above (Probe immobilization). The probes were striped by applying -1.0 V for 10 min in phosphate buffer. The stripped probes were quantified using qPCR.

MCH Backfilling. Typically, solution of 0.1 mM of MCH was prepared in 1mM Tris-Cl buffer for backfilling. The immobilized chips were washed in 1 mM Tris-Cl buffer for 5 min and immersed in MCH solution for 10 min under constant stirring. The chip was then washed 1 mM Tris-Cl buffer for 5 min. To study the effect of backfilling, MCH concentrations were changed from 0 (no backfilling) to 2.5 mM in the same buffer.

Scanning Electrometer for Electrical Double-layer (SEED). The primary electrochemical analysis was performed by SEED as briefly described in SI, Section S3 and Figure S2 (Vajra Instruments, USA). The CV ramp for SEED was -0.5 to +0.1 V at a scan rate of 1 V/s and step size of 24 mV with respect to Ag/AgCl reference electrode. A periodic AC potential of frequency, ω = 200 Hz at an amplitude of 100 mV was added to the CV ramp. The raw data was acquired by in-house software in Python scripts. The data was analyzed by MATLAB software (Mathworks, USA). The mathematical model, optical set-up and electronics instrumentation is described in a previous publication.[38]

Hybridization. The binding to probes (SI, Table S1) with specific and non-specific targets (SI, Table S2) were performed in 1X-MPBS at room temperature. Typically, the generic non-specific probe for control was Pcel39a. The specific probes and targets are noted in the respective parts of the study, for example, P34a and P155 in Figure 4a, and 20 nM T34a for prehybridization in Figure 6. A separate chip was used for each T34a concentration of 0.01 fM to 100 pM. For prehybridization and post-prehybridization, the binding time was 60 min and 180 min, respectively. The chip were washed in fresh 1X-MPBS to remove the adsorbed/unbound target molecules.

RESULTS AND DISCUSSION

An array of 25 microwells of 200 μm diameter were patterned on each of the three Au electrodes of a 1 cm^2 chip by photolithography (see Experimental Section). The ssDNA probes were spotted on each microwell using a home-built spotter; where, the volume of the probe solution droplet of ~0.5 nL and alignment on the microwell was spontaneously controlled by surface tension (SI, Figure S1). The probes with -SH terminal were immobilized to the electrode via well-known Au-S bind by incubation for 90 min in a humid environment at 21 ^{O}C to ensure no evaporation of the drop during the process (see Experimental Section). The probes had the generic formula of 3'-MB-[DNA]-$(CH_2)_6$-SH (SI, Table S1). The ssDNA sequences for study emulates miRNA circulating in the human blood that are promising biomarkers for early detection of cancer as referenced in SI, Table S1. For example, probe, P34a is DNA equivalent of compliment to miR34a where the uracil are replaced with thymine bases. Three specific target sequences, miR155, 34a and 92b were selected for the study (SI, Table S2). The sequences

chosen covered the typical range of GC fraction of 35 to 70% typically found in human miRNA.[39] Subsequently, the chip was backfilled using MCH to passivate the exposed Au electrode. The primary study is on miR34a using specific target, T34a.

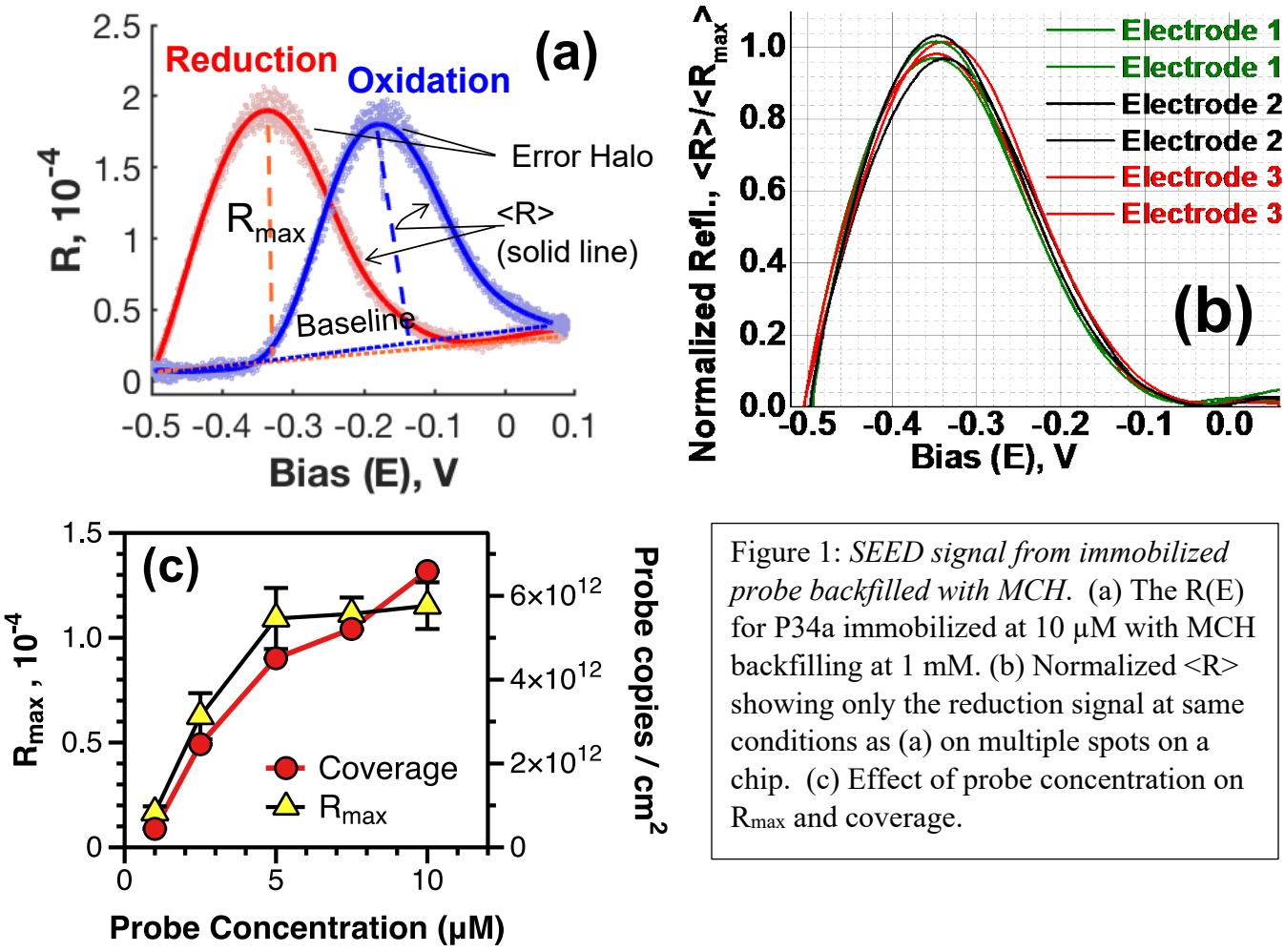

Figure 1: *SEED signal from immobilized probe backfilled with MCH.* (a) The R(E) for P34a immobilized at 10 μM with MCH backfilling at 1 mM. (b) Normalized <R> showing only the reduction signal at same conditions as (a) on multiple spots on a chip. (c) Effect of probe concentration on R_{max} and coverage.

The local redox of the tethered MB on each microwell was measured by differential reflectivity of a ~10 μm diameter laser beam during cyclic voltammetry (CV). The principle and set-up of the home built reflectometer called Scanning Electrometer for Electrical Double-layer (SEED) described earlier[38] is outlined in SI, Section S3 and Figure S2. Briefly, in SEED, a small AC potential of 100 mV amplitude at frequency, ω = 200 Hz was applied as the CV potential, E is periodically ramped between -0.5 to 0.1 V relative to Ag/AgCl reference electrode. The signal from SEED is the amplitude of reflectivity, R oscillating at ω, as the E is cycled over time, t (SI, Figure S3). The response for all the roughly eight CV cycles were superimposed to obtain an average <R> as a function of E, and the error halo was due to small cycle-to-cycle variations (Figure 1a). The peaks in <R> (and R) correspond to oxidation and reduction of MB. Due to the rapid exchange of electrons with the electrode compared to the slow diffusion of ions to compensate the imbalance, the electrical double layer (EDL) is unable to screen the charge leading to enhancement in ion oscillation causing the peaks.[38, 40] As the higher order harmonics

at 2ω was 10^3 fold lower, the system was linear. Thus, from electrostatics,[38] and also confirmed experimentally, the peak <R>, R_{max}, scales linearly with the peak current, I_{max}.[38, 41] As MB reduces to lucomethylene blue, for this study, we chose the reduction peak for R_{max}. The spot to spot variation between the three electrodes on the chip was small indicating fairly uniform coverage by individual spotting (Figure 1b). As expected, the R_{max} and probe coverage increased with probe concentration (Figure 1c). For the probe coverage, the Au-S bond were electrochemically cleaved, and the absolute copy number was determined by quantitative PCR (qPCR) as described in an earlier study.[38] Probe concentration of 10 µM was used in the study that yielded fairly stable R_{max} (being in the plateau region) with coverage of ~$6x10^{12}$ ssDNA/cm^2.

The effect of MCH concentration for backfilling revealed unexpected and surprising results that became the genesis of this study leading to a strategy to improve the LOQ. Three probes of different GC fraction from 37.5 to 72.7 % were immobilized individually on 25 microwells of each of the three respective electrodes of the chip. The backfilling was regulated by changing the MCH concentration for fixed exposure time of 10 min in a well stirred solution. For robust statistics, one spot on each microwell was measured to obtain 25 readings of R_{max} for each sequence. The R_{max} as a function of MCH concentration had two salient observations (Figure 2a). First, surprisingly, on no backfilling, i.e., MCH concentration of zero, the R_{max} was zero irrespective of the sequence (Figure 2a). Typical <R> for just the MB reduction for various MCH concentration clearly show that for no backfilling, there was no redox peak for MB (Figure 2b). Other sequences show similar behavior (SI, Figure S4). Differential pulse voltammetry (DPV) also shows no redox at no backfilling (SI, Figure S5). As per the prevailing explanation of electrochemical beacon, if there is no backfilling the MB at free-end should undergo redox with no hinderance.[5, 35] Second, also not an intuitive observation is that there is significant dependence on the sequence. As GC fraction increases the R_{max} generally increases. As all the three chains are of similar length, the chain flexibility should not change significantly due to differences in the sequences, thus, based on prevailing mechanism, there should not be a significant difference. The GC fraction effect was further explored by including six other sequences (see SI, Table S1) to find a systematic trend (Figure 2c) for backfilling with MCH concentration of 0.1 mM.

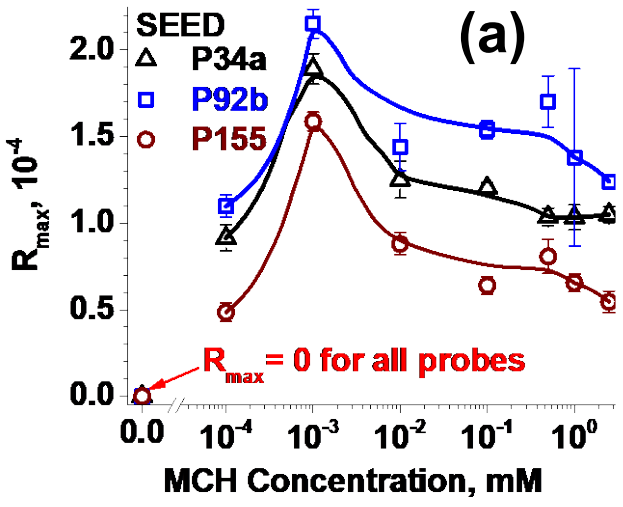

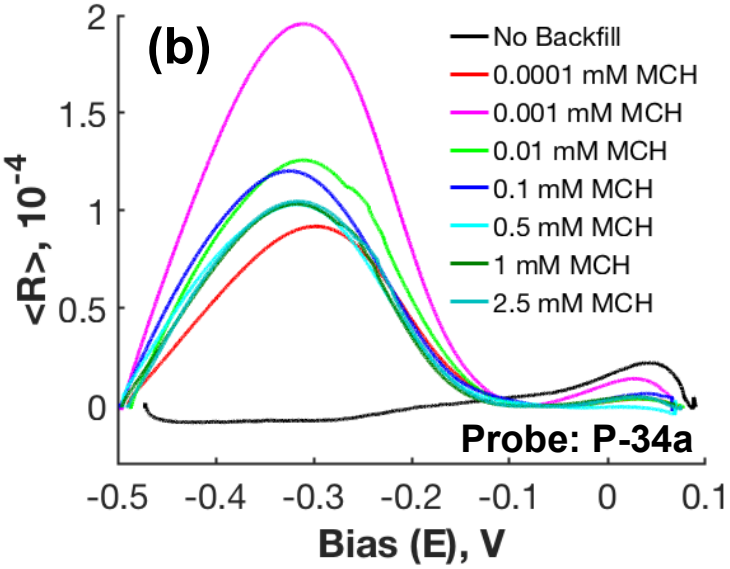

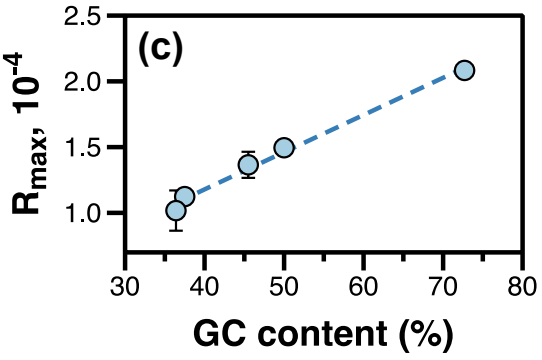

Figure 2: *Effect of MCH backfilling and probe on R_{max}*. (a) Change in R_{max} as a function of level of backfilling regulated by MCH concentration. To note is no redox peak is observed for no backfilling. (b) Typical E versus <R> for various levels of backfilling. The data is from different chips. The <R> is corrected for baseline. (c) The effect of sequence on the R_{max} signal at probe immobilization and backfilling conditions as Figure 1a.

An optimum MCH concentration for backfilling for our fixed backfilling process time of 10 min was in 0.01 to 0.5 mM range where R_{max} is reasonably constant (Figure 2a and SI, Figure S5). We fixed the MCH concentration at 0.1 mM for the study. At higher concentrations, due to higher backfilling density overcrowding effects occur leading to decrease in R_{max} (Figure 2a) and DPV (SI, Figure S5). We note that, although conventional electrochemical characterization, such as CV, DPV and AC Voltammetry are quantitatively consistent with SEED,[38, 41-43] we (currently) do not understand, the absence of peak at 1 μM in DPV (SI, Figure S5) as observed in SEED (Figure 2a).

To explain the unexpected observations, we start by considering the electrochemical potential of the system as it undergoes various surface modifications. A convenient visual approach is to consider the Fermi level (FL), or the energy , U of the negative charge (usually electron), i.e., as system charges negatively, the FL will rise (Figure 3a). Fermi level and electrochemical potential are equivalent.[44] For convenience, the buffer is grounded, which is typically the case in electrochemical measurements (Figure 3a): (i) Before contact the FL of Au is lower due its high work function. The difference in the FL before contact is PZC.[43, 45] (ii) As the Au electrode is immersed in the buffer solution containing ssDNA probe with MB, the FL of the electrode rises by accumulating negative charge.[45] Owing to their higher concentration and mobility, the buffer anions accumulate more to bring the FL in the equilibrium. As a result, even though the negatively charged tethered ssDNA probes are in the vicinity, most of them will stand-up as the FL is already in equilibrium due to the anions from the buffer. (iii) On MCH backfilling, majority of the buffer anions are displaced due to the strong Au-S bond of MCH. As a result, the negatively charged ssDNA will commence to come down to compensate for the loss in charge to stay in equilibrium. As a result, there will be a distribution where most probes are still up while some will be down. We note here that although this distribution should come to an equilibrium, in our experience it is very slow, usually over a day, thus the system is usually "frustrated" with a large variation (as will be described later in Figure 4b). (iv) If an external potential, E, relative to the buffer is applied, the FL of the Au electrode will shift. For $E > 0$, past PZC (i.e., $E > \phi$), the electrode will move down shedding all the anions and consequently repelling the ssDNA probe to stand-up. As a result, with PZC for Au electrode at ~+0.3 V relative to Ag/AgCl,[43, 45] the probes will stand-up.

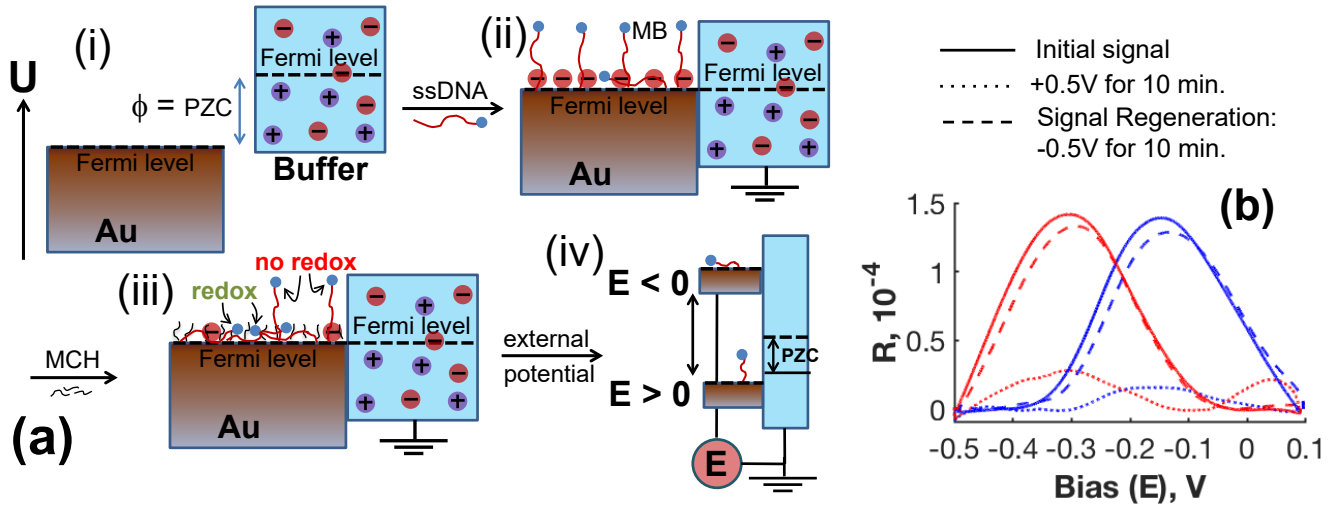

Figure 3: *State of immobilized probe due to backfilling and potential*. (a) The relative Fermi level of the electrode with respect to the electrode and change in probe conformation, (i) before electrode contacts the solution, (ii) after ssDNA probe immobilization, (iii) after backfilling, and (iv) due to external potential, E. The steps (ii) to (iv) are with electrode in the solution. (b) Effect of external potential on the redox signal for P34a immobilized and backfilled at conditions similar to Figure 1a. The R is corrected for baseline.

To explain the unexpected observations in Figure 2 in terms of electrostatics (Figure 3a), we propose that MB at the free-end undergoes redox only when the ssDNA probe is adsorbed on Au electrode (schematically indicated in Figure 3a-iii). The conjecture that redox of MB only occurs when the chains are down is supported by two observations: First, it is consistent with no signal for no back filling (Figure 2a, 2b and SI, Figure S5) when most of the chains are up (Figure 3a-ii). Second, on application of +0.5V, i.e., E > 0, the chains will stand-up (Figure 3a-iv) causing a decrease in redox signal of MB (Figure 3b). Furthermore, as -0.5V was applied, i.e., E < 0, the chains will come down again (Figure 3a-iv) explaining the reverting to the original value. Next, building on the proposed mechanism for MB redox, we developed the electrochemical beacon method for the simplest configuration where the target is nominally the same size as the probe.

We tested for specificity, as it is the minimum requirement to measure biospecimen. For a chip with P34a and P155 probes on the same electrode, we tested the binding to 100 nM T34a target. The redox of MB for specific binding vanished while for the non-specific probe the signal was unchanged indicating no binding (Figure 4a). Thus, the specificity is high. The decrease in R_{max} on binding is explained as follows: Before binding, the signal is from the probes that are down. These probes are adsorbed on the electrode due to the well documented strong interaction between Au with the bases.[46, 47] On probe-target binding, the bases will unbind from Au as they are folded inside the double helix. Due to the thermal motion of the rigid dsDNA, the anions from the solution will replace the charge on the electrode to compensate for the (lost) negative charge from the probe ssDNA. As a result, the chain will stand-up on binding. Thus, on binding, the redox signal will vanish causing the overall signal to drop. As the interaction of bases with Au depends on the sequence,[46, 47] this mechanism also qualitatively explains the GC dependence on the R_{max} shown in Figure 2c.

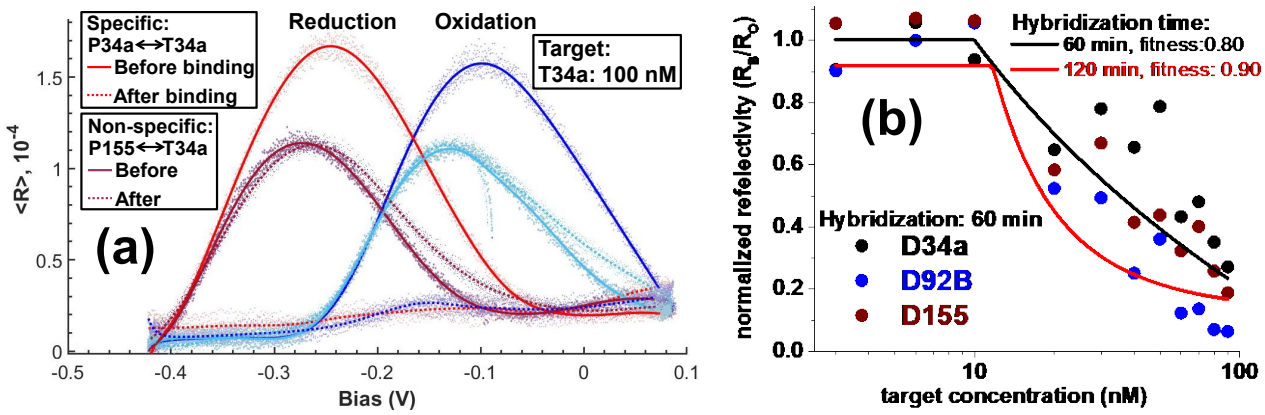

Figure 4: *Effect of high target concentration binding*. (a) Change in <R> (with error-halo) for P34a and P155 probes on binding to 100 nM target T34a. Both the probes are immobilized on the same electrode. The legend is for reduction peaks only. (b) Change in the reduction peak on binding to specific target, T34a at concentration 3 nM to 100 nM. The probe immobilization and backfilling conditions are same as Fig. 1(a).

The relative decrease in R_{max} before (R_O) and after binding (R_B) was studied as a function of target concentration, T34a (Figure 4b). The length of T34a is similar to P34a (SI, Table S1). For binding time of 60 min, insignificant change in the redox signal was observed at target concentrations below 10 nM. Thereafter, the signal decreases rapidly. Importantly, the decreases in the R_B /R_O exhibited significant scatter with no particular systematics with respect to GC fraction as was the case before binding (in Figure 2). Each data point for 60 min binding time was averaged over three readings on different microwells with R_B and R_O measured on the same respective microwell. Furthermore, the characteristics for binding time of 120 min was similar including the large scatter (data points shown in SI, Figure S6). The proposed mechanism points to an intrinsic challenge: As the probes that are up would be more prone to binding but will lead to no change in the redox signal. A change (i.e., decrease) in R_{max} will occur only when the binding is with chains that are down. As the majority of probes are up (Figure 3a-iii) the threshold to affect change in signal required large concentration of target (Figure 4b). As the distribution of up versus down probe chains was difficult to control as noted above as "frustrated distribution" in Figure 3a-iii due to slow kinetics, the change in signal was noisy (Figure 4b and SI, Figure S6).

We propose a simple, novel strategy of a "pre-hybridization" step to leave only adsorbed probes to bind to the target, as a result, both sensitivity will be improved, and the scatter will be reduced. The process is as follows (Figure 5): Based on the proposed mechanism (Figure 3a-ii), after immobilization very few probes are down (i.e., schematically, only P7 in Figure 5–i) leading to $R_{max} = 0$ (Figure 2a). On MCH backfilling the anions of the solution are displaced by MCH causing some chains to come down (Figure 3a-iii) that are schematically P4, P6, P7, and P9 (Figure 5-ii). On prehybridization with a large enough number of specific targets, all the probes standing up, i.e., P2, P3, P5, and P8 will bind (Figure 5-ii). Owing to large scatter of up/down

distribution, the concentration of target for prehybridization will be beyond the threshold, for example, 20 nM (Figure 4b). Few adsorbed targets, such as P9, will also bind and stand-up during prehybridization (Figure 5-iii). The optimization of prehybridization step (SI, Figure S7) indicates that 20 nM of specific target for 1 hour is sufficient to hybridize all up-probe chains (Figure 5-iii). Now the chip is primed to bind to the target where the only probes available for binding are all down. As a result, the targets will exclusively bind to probed that are down (such as, P6 and P7) resulting in a decrease in redox signal as the duplex stands-up (Figure 5-iv).

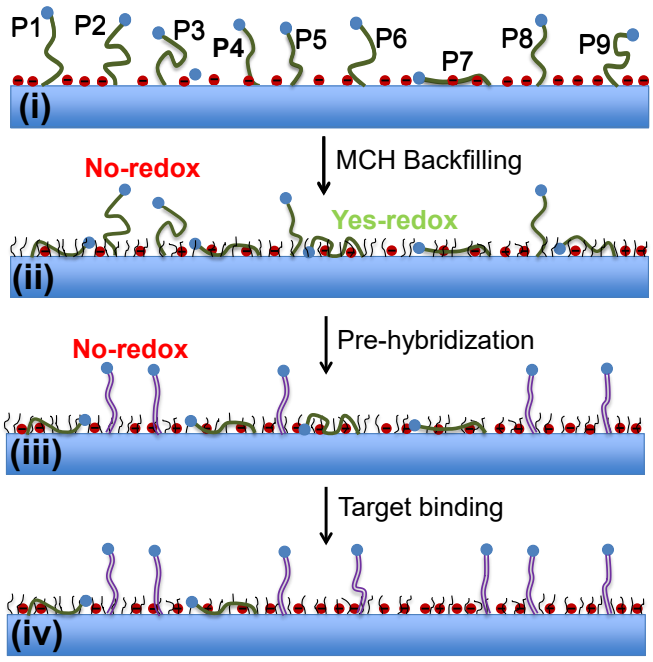

Figure 5: *The prehybridization method*. Schematic representation of probe conformation from immobilization to binding. Nine probes, P1 to P9 are shown to qualitatively represent relative fraction of conformational change. (i) Before backfilling, anions (red dots) adsorb on Au causing most probes to stand up (only P7 is down). (ii) MCH backfilling displaces the anions, bringing some of the probes down (P1, P4, P6, P7 and P9). (iii) On pre-hybridization all the probes up and fraction of probe down form duplex (P2, P3, P5, P8 and P9). (iv) The only available probes for targets to bind are down causing them to stand-up (P6, P7). The probes standing up and duplex (that will all stand up) will not show MB redox according to the model.

The concept is illustrated for binding with of 0.1 fM T34a target to immobilized probe P34a. Two conditions are compared, where the probes on one electrode are directly exposed to the target versus the probes on the other electrode (on the same chip) are primed by prehybridization before target binding (Figure 6a). For the probes not subject to prehybridization, consistent with previous reported methods,[3, 28, 29, 35] no change in R_{max} occurred. However, when the probe was prehybridized with 20 nM of target there was a remarkable change in signal by ~30% due to binding with 0.1 fM target. The prehybridization concentration being above the threshold (Figure 4b) leaves probes that adsorbed (as in Figure 5-iii) which leads to change in signal even with 0.1

fM target. As a comparison, the ~30% drop in prehybridized chip by 0.1 fM target (Figure 6a) is equivalent to 20 nM target required for the same drop without prehybridization (Figure 4b). Thus, prehybridization improves the sensitivity by eight orders of magnitude.

Next, we consider quantification. The large variation in R_{max} after pre-hybridization, i.e., R_B is inevitable (i.e., Figure 4b). The large scatter in R_B occurs in spite of initial fairly uniform distribution of up versus down probes before binding (i.e., Figure 1b). However, if the number of probes that are adsorbed are sufficient after pre-hybridization, i.e., $R_B \sim 1x10^{-4}$ (as in Figure 6a) we have adequate range to engineer a viable quantitative method. To compensate for the large scatter in R_{max} after pre-hybridization (i.e., R_B), the R_{max} on subsequent binding to the target (post pre-hybridization), R_f, was normalized as, R_f/R_B. To study the effect of sequence, three sequences covering G-C fraction from 37.5% to 72.7% were studied (Figure 6(b)). The <R> normalized by R_B was well above the noise level for a broad target concentration. Typical normalized <R> showing systematic change on binding for all the three sequences are shown in SI for each of the target concentration (SI, Figure S8). The R_f/R_B were quantitative, exhibiting a highly linear signal on a semi-log plot over the entire range (Figure 6(b)). The resulting LOQ was 10 attomolar (aM) and the dynamic range was seven orders of magnitude. Each data point was averaged over six microwells on the same chip. The error bars were very small. The chip also had control on each of the electrode with probes that were non-specific to the target to ensure specificity. The non-specific probes for T34a were P155, P92b and Pcel39a, while for the other two targets the controls were the (other) two non-complimentary probes and Pcel39a. We note that at high G-C% of 72%, i.e., P92b, the LOQ was 100 aM. We conjecture that the lower LOQ was due to poor binding efficiency owing to the strong adsorption of the probe to the Au electrode due to high G-C fraction (Figure 2(c)). To quantify change in binding efficiency on G-C fraction, unfortunately, the binding constant, unlike for fluorescence-based systems,[48] is difficult. Primarily because, binding to probes that are up will lead to no change in signal while the ones down will lead to a change in signal (as noted in Figure 5(iii) and experimentally shown in Figure 6(a)). To independently measure the binding constant for up versus down probes that will be different requires concomitant measurement of structure in real time to follow the kinetics. Although, structural heterogenous complexity of the immobilized film (i.e., Figure 5) makes binding constant measurement difficult, the systematics is robust as evident from the tight error bar (Figure 6(b)). The calibration curve for T155 and T43a being nominally coincident suggests that below 50% G-C fraction, the desorption of the probe to bind is the rate determining step rather than the hybridization kinetics.

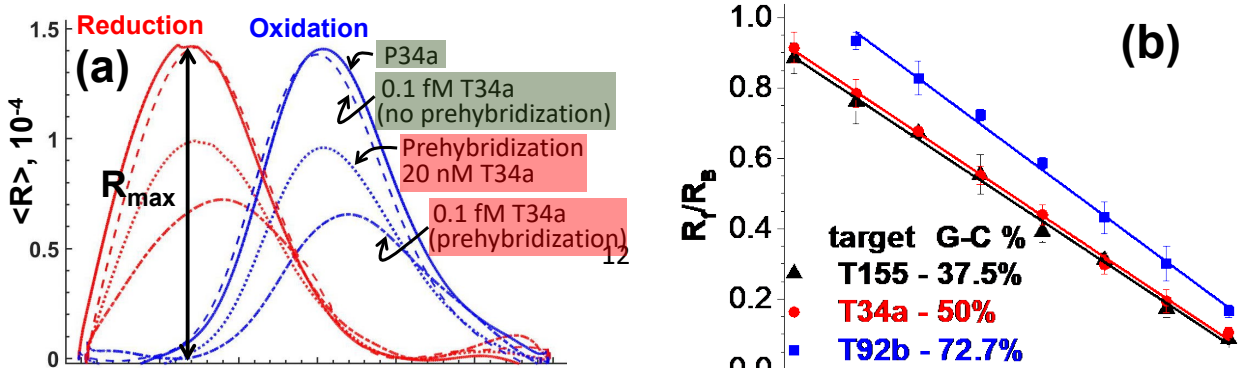

Figure 6: *Quantification of target*. (a) The effect of prehybridization showing the enhancement in sensitivity. (b) The systematic decrease in signal due to binding with target after prehybridization. The fitness for all the curves is in 0.984 to 0.985 range. The error bar was based on six independent spots.

SUMMARY

In summary, we have proposed a strategy to improve the performance of electrochemical beacon method by prehybridization to achieve LOQ of 10 aM and a dynamic range of seven orders of magnitude. For the study, ~25 nucleotide probes of ssDNA with MB at 3'-end were tethered on the Au electrode at 5'-end via thio-linkage followed by backfilling with MCH. The binding with similar length of target was measured as decrease in the redox peak of tethered MB. The prehybridization approach was based on two observations: First, for no backfilling there was no MB redox even though there was complete accessibility to the underlying Au electrode. Second, the MB redox strongly depend on the probe sequence. The results suggest that MB redox exclusively occurs when the chain is adsorbed to the surface due to strong interaction between the bases and Au. On binding if the probe is already standing up no change in signal will occur. However, if the probe is adsorbed the interaction with the base is broken and the duplex stands-up resulting in decrease in signal. Therefore, the strategy was to prime the chip by prehybridizing with large amount of specific target so that the probes standing up will bind first leaving only the adsorbed probes. As a result, when the targets bind to a prehybridized chip, the redox signal changes significantly with only 10 aM target concentration compared to nanomolars for similar change in chip that was not primed. The redox of MB was measured by a home built differential reflectometer called SEED that allowed reading on multiple 10 μm spots on a monolith electrode. An LOQ and dynamic range of 10 aM and seven orders of magnitudes was obtained for G-C fraction up to 50%. The LOQ reduced to 100 aM for G-C fraction of 72%. The combination of prehybridization with multiplexing on a monolith electrode by SEED, the findings will allow the development of label-free, enzyme-free, electrochemical DNA and RNA probe microarray chip technology to quantify a variety of molecules including nucleic acids and proteins on a monolith electrode in attomolar to picomolar range.

ASSOCIATED CONTENT

Supporting Information

The Supporting Information is available for free of charge on the ACS Publications website.

The SI has seven, two tables and eight figures covering, details on chip spotting, probe and target sequences, SEED set-up and signal, optimization of MCH backfilling (DPV and SEED) and prehybridization, effect of binding time, signals to specific binding, and sensitivity analysis of prehybridization on different GC fraction sequences.

Author Information

Corresponding Authors

*E-mail: rsaraf2@unl.edu; rahul.tevatia@vajrainstruments.com

ORCID

Ravi F. Saraf: 0000-0002-8537-054X

Rahul Tevatia: 0000-0002-6783-5649

NOTES

Ravi F. Saraf discloses financial interest in Vajra Instrument as its founder and President.

ACKNOWLEDGMENTS

RFS thanks National Cancer Institute of the National Institutes of Health, USA for financial support (2R44CA199058).

REFERENCES

1. Campuzano, S.; Yanez-Sedeno, P.; Pingarron, J. M., Tailoring Sensitivity in Electrochemical Nucleic Acid Hybridization Biosensing: Role of Surface Chemistry and Labeling Strategies. *ChemElectroChem* **2019,** *6* (1), 60-72.
2. Pellitero, M. A.; Shaver, A.; Arroyo-Currás, N., Critical Review—Approaches for the Electrochemical Interrogation of DNA-Based Sensors: A Critical Review. *J. Electrochem. Soc.* **2020,** *167* (3), 037529.
3. Fan, C.; Plaxco, K. W.; Heeger, A. J., Electrochemical interrogation of conformational changes as a reagentless method for the sequence-specific detection of DNA. *Proc. Natl. Acad. Sci. U.S.A.* **2003,** *100* (16), 9134-9137.
4. Idili, A.; Amodio, A.; Vidonis, M.; Feinberg-Somerson, J.; Castronovo, M.; Ricci, F., Folding-Upon-Binding and Signal-On Electrochemical DNA Sensor with High Affinity and Specificity. *Anal. Chem.* **2014,** *86* (18), 9013-9019.
5. Dauphin-Ducharme, P.; Arroyo-Curras, N.; Plaxco, K. W., High-Precision Electrochemical Measurements of the Guanine-, Mismatch-, and Length-Dependence of Electron Transfer from Electrode-Bound DNA Are Consistent with a Contact-Mediated Mechanism. *J. Am. Chem. Soc.* **2019,** *141* (3), 1304-1311.
6. Han, K.; Liang, Z.; Zhou, N., Design strategies for aptamer-based biosensors. *Sensors (Basel)* **2010,** *10* (5), 4541-4557.
7. Hai, X.; Li, Y.; Zhu, C.; Song, W.; Cao, J.; Bi, S., DNA-based label-free electrochemical biosensors: from principles to applications. *Trends Analyt. Chem.* **2020**, 116098.
8. Yoo, H.; Jo, H.; Oh, S. S., Detection and beyond: challenges and advances in aptamer-based biosensors. *Mater. Adv.* **2020,** *1* (8), 2663-2687.

9. Wang, L.; Peng, X.; Fu, H.; Huang, C.; Li, Y.; Liu, Z., Recent advances in the development of electrochemical aptasensors for detection of heavy metals in food. *Biosens. Bioelectron.* **2020,** *147*, 111777.
10. Yang, Y.; Li, W.; Liu, J., Review of recent progress on DNA-based biosensors for Pb(2+) detection. *Anal. Chim. Acta* **2021,** *1147*, 124-143.
11. Abu-Ali, H.; Nabok, A.; Smith, T. J., Development of novel and highly specific ssDNA-aptamer-based electrochemical biosensor for rapid detection of mercury (II) and lead (II) ions in water. *Chemosensors* **2019,** *7* (2), 27.
12. Selvolini, G.; Băjan, I.; Hosu, O.; Cristea, C.; Săndulescu, R.; Marrazza, G., DNA-Based Sensor for the Detection of an Organophosphorus Pesticide: Profenofos. *Sensors (Basel)* **2018,** *18* (7), 2035.
13. Phopin, K.; Tantimongcolwat, T., Pesticide Aptasensors—State of the Art and Perspectives. *Sensors* **2020,** *20* (23), 6809.
14. Ferreira, D. C.; Batistuti, M. R.; Bachour, B.; Mulato, M., Aptasensor based on screen-printed electrode for breast cancer detection in undiluted human serum. *Bioelectrochemistry* **2020,** *137*, 107586.
15. White, R. J.; Phares, N.; Lubin, A. A.; Xiao, Y.; Plaxco, K. W., Optimization of electrochemical aptamer-based sensors via optimization of probe packing density and surface chemistry. *Langmuir* **2008,** *24* (18), 10513-10518.
16. Liu, Y.; Tuleouva, N.; Ramanculov, E.; Revzin, A., Aptamer-Based Electrochemical Biosensor for Interferon Gamma Detection. *Anal. Chem.* **2010,** *82* (19), 8131-8136.
17. Song, Y.; Song, J.; Wei, X.; Huang, M.; Sun, M.; Zhu, L.; Lin, B.; Shen, H.; Zhu, Z.; Yang, C., Discovery of Aptamers Targeting the Receptor-Binding Domain of the SARS-CoV-2 Spike Glycoprotein. *Anal. Chem.* **2020,** *92* (14), 9895-9900.
18. Li, H.; Dauphin-Ducharme, P.; Ortega, G.; Plaxco, K. W., Calibration-Free Electrochemical Biosensors Supporting Accurate Molecular Measurements Directly in Undiluted Whole Blood. *J. Am. Chem. Soc.* **2017,** *139* (32), 11207-11213.
19. Li, H.; Arroyo-Currás, N.; Kang, D.; Ricci, F.; Plaxco, K. W., Dual-Reporter Drift Correction To Enhance the Performance of Electrochemical Aptamer-Based Sensors in Whole Blood. *J. Am. Chem. Soc.* **2016,** *138* (49), 15809-15812.
20. Ricci, F.; Lai, R. Y.; Heeger, A. J.; Plaxco, K. W.; Sumner, J. J., Effect of Molecular Crowding on the Response of an Electrochemical DNA Sensor. *Langmuir* **2007,** *23* (12), 6827-6834.
21. Hüsken, N.; Gebala, M.; Schuhmann, W.; Metzler-Nolte, N., A single-electrode, dual-potential ferrocene-PNA biosensor for the detection of DNA. *Chembiochem* **2010,** *11* (12), 1754-1761.
22. Radi, A.-E.; Acero Sánchez, J. L.; Baldrich, E.; O'Sullivan, C. K., Reagentless, Reusable, Ultrasensitive Electrochemical Molecular Beacon Aptasensor. *J. Am. Chem. Soc.* **2006,** *128* (1), 117-124.
23. Southern, E.; Mir, K.; Shchepinov, M., Molecular interactions on microarrays. *Nat. Genet.* **1999,** *21* (1), 5-9.
24. Peeters, S.; Stakenborg, T.; Reekmans, G.; Laureyn, W.; Lagae, L.; Van Aerschot, A.; Van Ranst, M., Impact of spacers on the hybridization efficiency of mixed self-assembled DNA/alkanethiol films. *Biosens. Bioelectron.* **2008,** *24* (1), 72-7.

25. Chen, H.; Meisburger, S. P.; Pabit, S. A.; Sutton, J. L.; Webb, W. W.; Pollack, L., Ionic strength-dependent persistence lengths of single-stranded RNA and DNA. *Proc. Natl. Acad. Sci. U.S.A.* **2012,** *109* (3), 799-804.
26. Herne, T. M.; Tarlov, M. J., Characterization of DNA Probes Immobilized on Gold Surfaces. *J. Am. Chem. Soc.* **1997,** *119* (38), 8916-8920.
27. Rant, U.; Arinaga, K.; Fujita, S.; Yokoyama, N.; Abstreiter, G.; Tornow, M., Dynamic Electrical Switching of DNA Layers on a Metal Surface. *Nano Lett.* **2004,** *4* (12), 2441-2445.
28. Rant, U.; Arinaga, K.; Scherer, S.; Pringsheim, E.; Fujita, S.; Yokoyama, N.; Tornow, M.; Abstreiter, G., Switchable DNA interfaces for the highly sensitive detection of label-free DNA targets. *Proc. Natl. Acad. Sci. U.S.A.* **2007,** *104* (44), 17364-17369.
29. Cai, Z. M.; Song, Y. L.; Wu, Y. F.; Zhu, Z.; Yang, C. J.; Chen, X., An electrochemical sensor based on label-free functional allosteric molecular beacons for detection target DNA/miRNA. *Biosens. Bioelectron.* **2013,** *41*, 783-788.
30. Rao, A. N.; Grainger, D. W., Biophysical properties of nucleic acids at surfaces relevant to microarray performance. *Biomater. Sci.* **2014,** *2* (4), 436-471.
31. Peterson, A. W.; Heaton, R. J.; Georgiadis, R. M., The effect of surface probe density on DNA hybridization. *Nucleic Acids Res.* **2001,** *29* (24), 5163-8.
32. Steel, A. B.; Herne, T. M.; Tarlov, M. J., Electrochemical Quantitation of DNA Immobilized on Gold. *Anal. Chem.* **1998,** *70* (22), 4670-4677.
33. Gong, P.; Levicky, R., DNA surface hybridization regimes. *Proc. Natl. Acad. Sci. U.S.A.* **2008,** *105* (14), 5301-5306.
34. Irving, D.; Gong, P.; Levicky, R., DNA Surface Hybridization: Comparison of Theory and Experiment. *J. Phys. Chem. B* **2010,** *114* (22), 7631-7640.
35. Xiao, Y.; Lubin, A. A.; Baker, B. R.; Plaxco, K. W.; Heeger, A. J., Single-step electronic detection of femtomolar DNA by target-induced strand displacement in an electrode-bound duplex. *Proc. Natl. Acad. Sci. U.S.A.* **2006,** *103* (45), 16677-16680.
36. Wang, T. Y.; Viennois, E.; Merlin, D.; Wang, G. L., Microelectrode miRNA Sensors Enabled by Enzyme less Electrochemical Signal Amplification. *Anal. Chem.* **2015,** *87* (16), 8173-8180.
37. Xia, F.; White, R. J.; Zuo, X. L.; Patterson, A.; Xiao, Y.; Kang, D.; Gong, X.; Plaxco, K. W.; Heeger, A. J., An Electrochemical Supersandwich Assay for Sensitive and Selective DNA Detection in Complex Matrices. *J. Am. Chem. Soc.* **2010,** *132* (41), 14346-14348.
38. Tevatia, R.; Prasad, A.; Saraf, R. F., Electrochemical Characteristics of a DNA Modified Electrode as a Function of Percent Binding. *Anal. Chem.* **2019,** *91* (16), 10501-10508.
39. Davis, N.; Biddlecom, N.; Hecht, D.; Fogel, G. B., On the relationship between GC content and the number of predicted microRNA binding sites by MicroInspector. *Comput. Biol. Chem.* **2008,** *32* (3), 222-226.
40. Raghunath, S.; Prasad, A.; Tevatia, R.; Gunther, J. R.; Roy, S.; Krishnan, S.; Saraf, R. F., Quantitative Electrochemical DNA Microarray on a Monolith Electrode with Ten Attomolar Sensitivity, 100% Specificity, and Zero Background. *Chemelectrochem* **2018,** *5* (3), 429-433.
41. Lee, S. W.; Lopez, J.; Saraf, R. F., Direct mapping of local redox current density on a monolith electrode by laser scanning. *Biosens. Bioelectron.* **2013,** *47*, 408-414.
42. Singh, G.; Moore, D.; Saraf, R. F., Localized Electrochemistry on a 10 mu m Spot on a Monolith Large Electrode: An Avenue for Electrochemical Microarray Analysis. *Anal. Chem.* **2009,** *81* (15), 6055-6060.

43. Saraf, A. R.; Keramatnejad, K.; Arcila, J. A.; Saraf, R. F., Electrostatics of Single Monolayer Graphene Coated Metal Electrode in Electrolyte. *Adv. Mater. Interfaces* **2021**, 8 (14) 2100370.
44. Reiss, H., The Fermi level and the redox potential. *J. Phys. Chem.* **1985,** *89* (18), 3783-3791.
45. Moore, D.; Arcila, J. A.; Saraf, R. F., Electrochemical Deposition of Polyelectrolytes Is Maximum at the Potential of Zero Charge. *Langmuir* **2020,** *36* (8), 1864-1870.
46. Brown, K. A.; Park, S.; Hamad-Schifferli, K., Nucleotide−Surface Interactions in DNA-Modified Au−Nanoparticle Conjugates: Sequence Effects on Reactivity and Hybridization. *J. Phys. Chem. C* **2008,** *112* (20), 7517-7521.
47. Koo, K. M.; Sina, A. A. I.; Carrascosa, L. G.; Shiddiky, M. J. A.; Trau, M., DNA–bare gold affinity interactions: mechanism and applications in biosensing. *Anal. Methods* **2015,** *7* (17), 7042-7054.
48. Zhou, M.; Chen, X.; Yang, H.; Fang, X.; Gu, H.; Xu, H., Determination of the Binding Constant between Oligonucleotide-Coupled Magnetic Microspheres and Target DNA. *ACS Omega* **2019,** *4* (4), 6931-6938.

Supporting Information

Electrochemical Beacon Method to Quantify Ten Attomolar of Nucleic Acids with Semi-Log Dynamic Range of Seven Orders of Magnitude

Rahul Tevatia[a],*, Alicia Chan[a], Lance Oltmanns[a], JayMin Lim[a], Ander Christensen[a], Michael Stoller[a], Ravi F. Saraf[b],[c],*

[a]Vajra Instruments, Lincoln, NE 68512, USA; [b]University of Nebraska, Lincoln, NE 68588, USA; [c]Nebraska Center for Material and Nanoscience, University of Nebraska-Lincoln, NE 68512
*rahul.tevatia@vajrainstruments.com; rsaraf2@unl.edu

SI Table of Contents **Page**

S1. Spotting of probes on electrodes with lithographed microwells

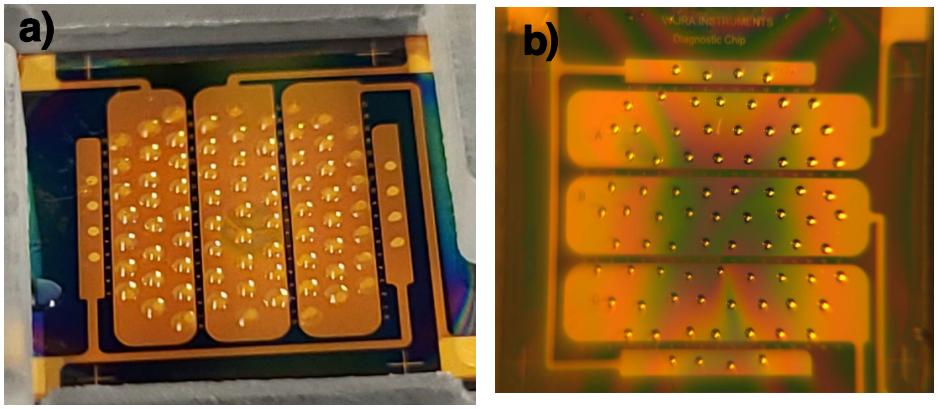

Figure S1. Different 10 µM probe solutions were spotted on 200 µm diameter microwells by a semi-automated spotter (Vajra Instruments Inc., USA). a) Vajra Instrument's customized chip with droplets of probe solutions defined by capillary force, b) top-view of a spotted chip in the camera used for spotting.

S2. Probe and target sequences

Table S1. Probes used to study the effect of GC content,[a] MCH backfill,[b] prehybridization,[c] and target hybridization.[d]

Probe	Sequence	Length	GC %	Tm (°C)	Significance (Biomarker)
P21[a]	5' SH-$(CH_2)_6$-TCAACATCAGTC TGATAAGCTA-MB 3'	22 nt	36.4	50.9	Cancer[1-3]
P34a[a-d]	5' SH-$(CH_2)_6$-ACAACCAGCTAA GACACTGCCA-MB 3'	22 nt	50	58.8	Cancer, Senescence[1-5]
P92b[a-c]	5' SH-$(CH_2)_6$-CACTGCACCGCG TCCCGTCCCT-MB 3'	22 nt	72.7	68.4	Cancer[1-3]
P141[a]	5' SH-$(CH_2)_6$-TCCAACACTGTA CTGGAAGATG-MB 3'	22 nt	45.5	54.3	Cancer, Melanogenesis, Chemotherapy[1-3, 6]
P155[a-c]	5' SH-$(CH_2)_6$-AACCCCTATCAC GATTAGCATTAA-MB 3'	24 nt	37.5	53.9	Cancer, Immune Thrombocytopenia[1, 2, 7, 8]
P451[a]	5' SH-$(CH_2)_6$-AACTCAGTAATG GTAACGGTTT-MB -3'	22 nt	36.4	52	Cancer[1, 2]
P630[a]	5' SH-$(CH_2)_6$-ACCTTCCCTGGT ACAGAATACT-MB 3'	22 nt	45.5	54.9	Cancer, Apoptosis, Chemotherapy[1, 9, 10]
Pcel39a[a,c-d]	5' SH-$(CH_2)_6$-TATTACCAAGAC GAAATCAGCT-MB 3'	22 nt	36.4	51.6	Negative Control for human miRNA microarray or qPCR

Table S2. Target sequence to study hybridization[a] and limit of quantification[b]

Target	Sequence	Length	GC %	Tm (°C)
T-34a [a,b]	5' TGGCAGTGTCTTAGC TGGTTGT 3'	22 nt	50	58.8
T-92b [a]	5' AGGGACGGGACGCGG TGCAGTG 3'	22 nt	72.7	68.4
T-155 [a]	5' TTAATGCTAATCGTG ATAGGGGTT 3'	24 nt	37.5	53.9

S3. SEED set-up and signal

A 2 mW He-Ne laser of beam diameter of ~10 µm is focused on the microwell spot. The electrode is subjected to a CV potential, E combined with an AC potential (Fig. S2). As a result of the AC potential at a frequency of ω, the amplitude of the reflected beam oscillates at ω. The oscillatory reflectivity is measured by a lock-in-amplifier tuned exactly at ω by the power supply. The resulting amplitude of the oscillatory reflectivity at ω is given by,[11]

$$R = \frac{R_A}{R_O} = 4n_2 \frac{(k_2^2 - \langle n_{1s}\rangle^2)}{(\langle n_{1s}\rangle^2 + k_2^2)^2_1} \delta n_s \qquad (1)$$

where, δn_s is the amplitude of refractive index oscillation that is spatially averaged over the interface, R_A and R_O are the amplitude of AC intensity at ω and the incident laser intensity (i.e., DC signal), respectively, measured at the detector; $n_2 - ik_2$ is the complex refractive index of the WE; and $\langle n_{1s}\rangle$ is the spatially averaged refractive index of the solution at the interface. The signal R as a function of E was obtained by normalizing the R_A measured by a lock-in-amplifier tuned at ω with R_O. The second harmonic signal by the lock-in-amplifier was three orders of magnitude lower than the first order, thus, the system was assumed to be linear (Eq. (1)). The primary principle of the measurement is that due rapid electron exchange with the electrode, the emanating field from the electrode is significantly enhanced leading to an increase in δn_s resulting in a peak.[11, 12]

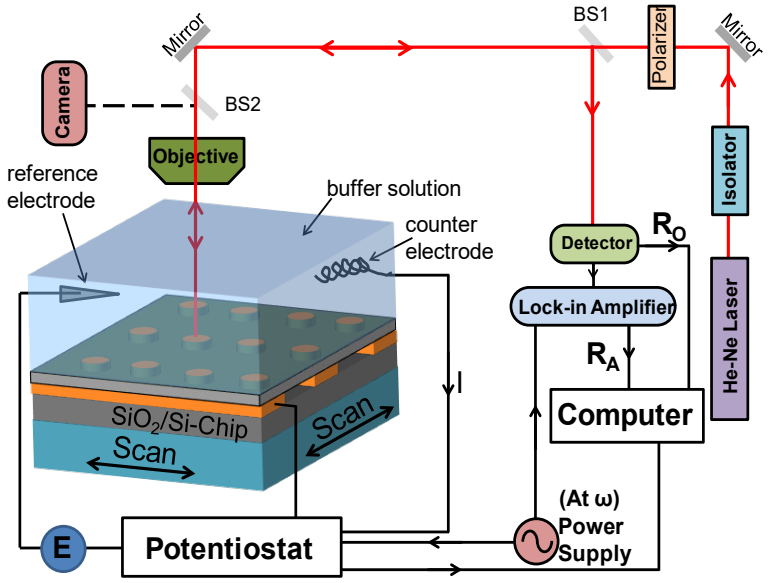

Figure S2. Schematic of SEED (Scanning Electrometer for Electrical Double Layer, Vajra Instruments Inc., USA). RE-Reference Electrode, WE-Working Electrode, and CE-Counter Electrode.

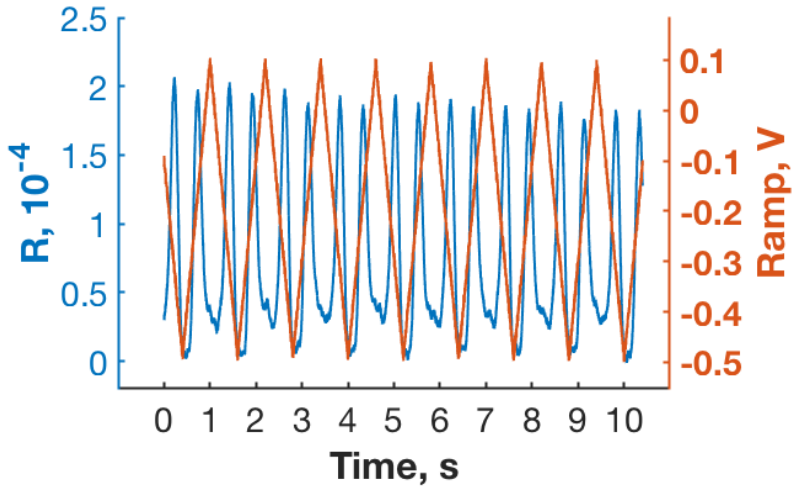

Figure S3. SEED raw data plot. The R (right, blue) and CV ramp potential, E in V (left, orange) as a function of time, t in s. The raw signal corresponds to P34a immobilized on a 200 µm-lithographed chip using immobilization and backfilling condition same as Fig. 1(a). The reduction and oxidation peaks are ramp down and up, respectively.

S4. Effect of MCH backfilling

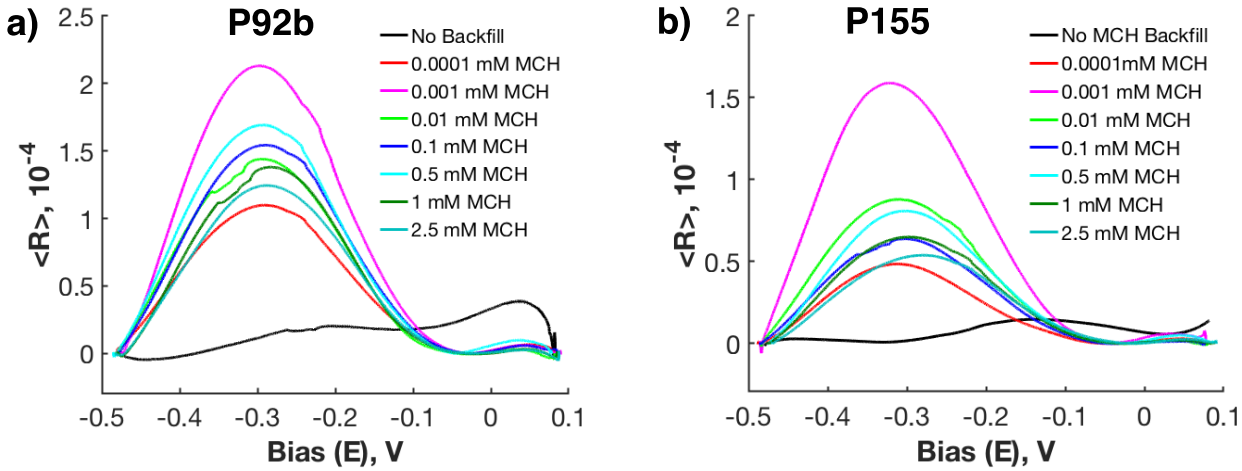

Figure S4. Reduction plots from SEED read for different MCH concentrations during backfill process on a) P92b, and b) P155. The concentration for immobilization for P92b and P155 were kept constant to 10 µM. The backfilling condition was similar to Fig. 1(a).

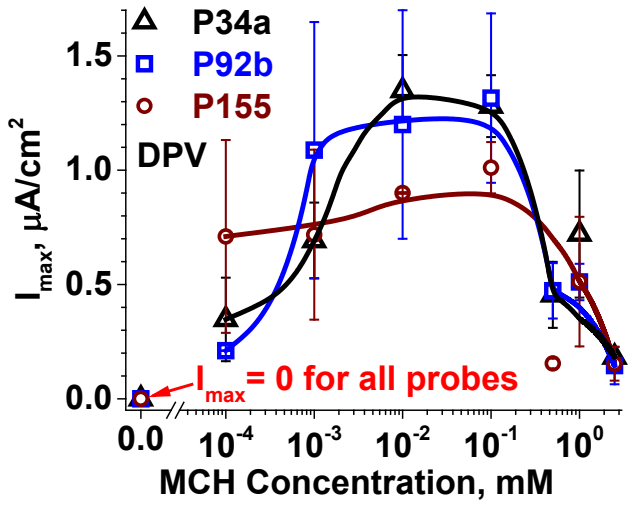

Figure S5. Differential Pulse Voltammetry (DPV) performed on an entire electrode with all 25 microwells immobilized with either of three probes P34a, P92b or P155 while varying the MCH backfill conditions. DPV was performed using Autolab NOVA 2.0 software on all of the electrodes with the following conditions: step = 0.005 V, modulation amplitude = 0.02 V, modulation time = 0.005 s; and interval time = 0.5 s.

S5. Effect of binding time of 120 min on R_{max}

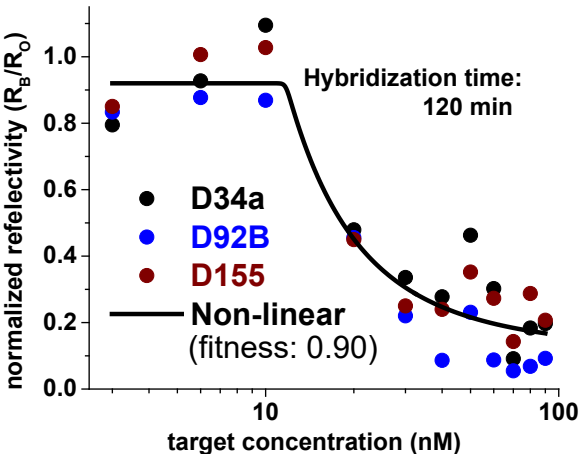

Figure S6. Similar to Fig. 4(b) in MS except the hybridization time was 120 min. Hybridization was performed with respective probes immobilized on lithographed chip in 1x-MPBS buffer (pH 7.2) for 120 minutes.

S6. Optimization of prehybridization method

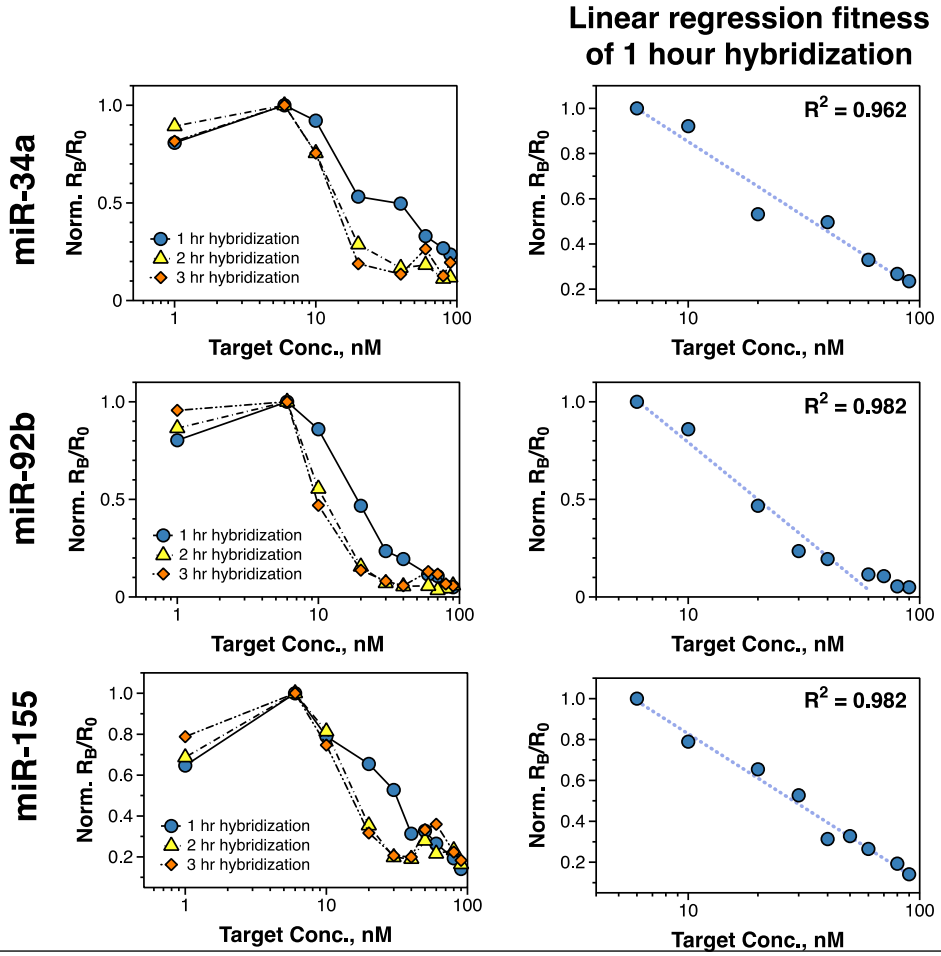

Figure S7. Optimization of prehybridization condition for miR-34a, 92b and 155 with their respective targets at three different time intervals– 1 hour, 2 hours, and 3 hours. Hybridization was performed with respective probes immobilized on lithographed chip in 1x-MPBS buffer (pH 7.2).

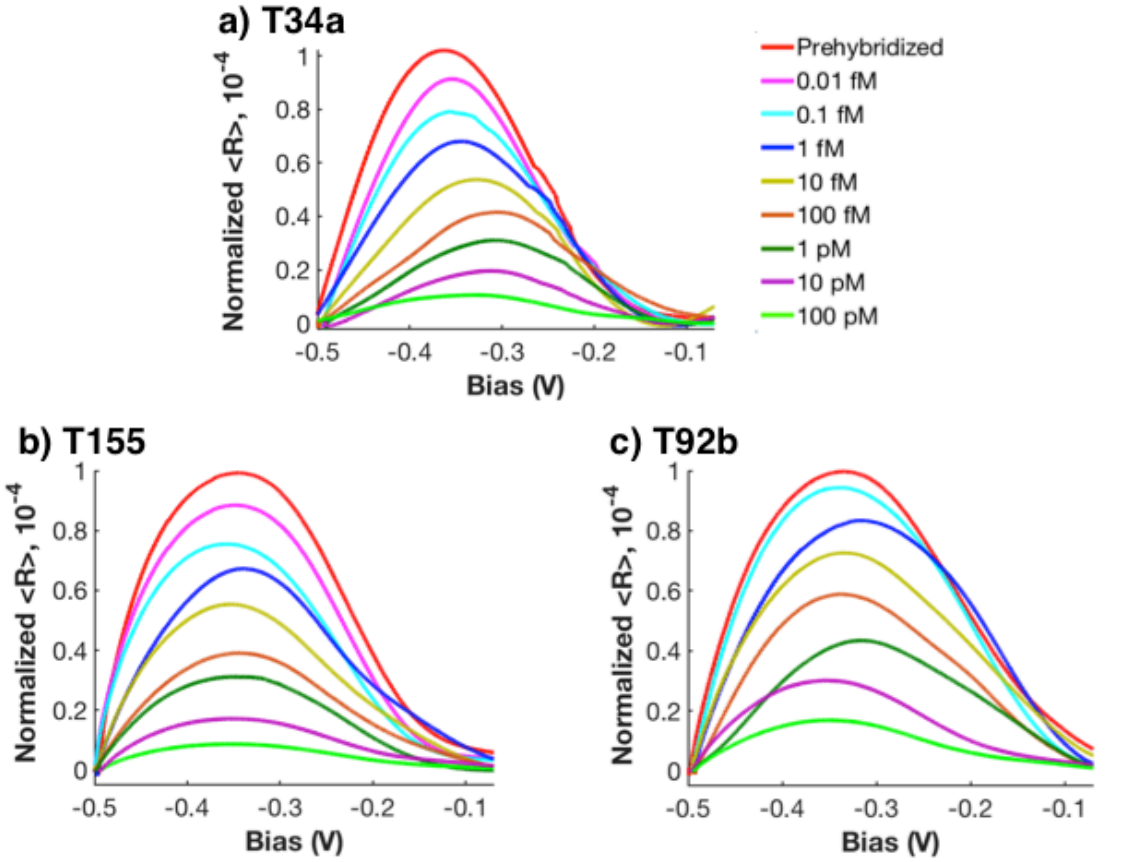

Figure S8. Typical normalized <R> for different target concentration for a) T34a, b) T155 and c) T92b. The <R> is normalized with to the corresponding R_{max} before binding (but after prehybridization) for each of the curves. In other words, the normalization is with respect to R_B in Fig. 6(b); and the R_{max} is R_f.

References

1. Bartel, D. P., MicroRNAs: Target Recognition and Regulatory Functions. *Cell* **2009,** *136*, 215-233.
2. Meng, F.; Henson, R.; Lang, M.; Wehbe, H.; Maheshwari, S.; Mendell, J. T.; Jiang, J.; Schmittgen, T. D.; Patel, T., Involvement of human micro-RNA in growth and response to chemotherapy in human cholangiocarcinoma cell lines. *Gastroenterology* **2006,** *130*, 2113-2129.
3. Yong, E., Cancer biomarkers: Written in blood. *Nature* **2014,** *511*, 524-526.
4. Hermeking, H., The miR-34 family in cancer and apoptosis. *Cell Death Differ.* **2010,** *17*, 193-199.
5. Mokhberian, N.; Bolandi, Z.; Eftekhary, M.; Hashemi, S. M.; Jajarmi, V.; Sharifi, K.; Ghanbarian, H., Inhibition of miR-34a reduces cellular senescence in human

adipose tissue-derived mesenchymal stem cells through the activation of SIRT1. *Life Sci.* **2020,** *257*, 118055.

6. Ye, Y.; Yuan, X.-H.; Wang, J.-J.; Wang, Y.-C.; Li, S.-L., The diagnostic value of miRNA-141 in prostate cancer: A systematic review and PRISMA-compliant meta-analysis. *Medicine* **2020,** *99*, e19993.
7. Chang, Y.; Chen, X.; Tian, Y.; Gao, X.; Liu, Z.; Dong, X.; Wang, L.; He, F.; Zhou, J., Downregulation of microRNA-155-5p prevents immune thrombocytopenia by promoting macrophage M2 polarization via the SOCS1-dependent PD1/PDL1 pathway. *Life Sci.* **2020,** *257*, 118057.
8. Tam, W.; Dahlberg, J. E., miR-155/BIC as an oncogenic microRNA. *Genes Chromosomes Cancer* **2006,** *45*, 211-212.
9. Chu, D.; Zhao, Z.; Li, Y.; Li, J.; Zheng, J.; Wang, W.; Zhao, Q.; Ji, G., Increased microRNA-630 expression in gastric cancer is associated with poor overall survival. *PLoS One* **2014,** *9*, e90526.
10. Eoh, K. J.; Lee, S. H.; Kim, H. J.; Lee, J.-Y.; Kim, S.; Kim, S. W.; Kim, Y. T.; Nam, E. J., MicroRNA-630 inhibitor sensitizes chemoresistant ovarian cancer to chemotherapy by enhancing apoptosis. *Biochem. Biophys. Res. Commun.* **2018,** *497*, 513-520.
11. Tevatia, R.; Prasad, A.; Saraf, R. F., Electrochemical Characteristics of a DNA Modified Electrode as a Function of Percent Binding. *Anal. Chem.* **2019,** *91*, 10501-10508.
12. Raghunath, S.; Prasad, A.; Tevatia, R.; Gunther, J. R.; Roy, S.; Krishnan, S.; Saraf, R. F., Quantitative Electrochemical DNA Microarray on a Monolith Electrode with Ten Attomolar Sensitivity, 100% Specificity, and Zero Background. *Chemelectrochem* **2018,** *5*, 429-433.